CAMKK2 promotes prostate cancer independently of AMPK via increased lipogenesis

Lucy Penfold[1], Angela Woods[1], Phillip Muckett[1], Alexander Yu. Nikitin[2], Tera R. Kent[2], Shuai Zhang[1], Rebecca Graham[1], Alice Pollard[1] and David Carling[1,3]

[1]MRC London Institute of Medical Sciences, Imperial College London, Hammersmith Hospital, London W12 0NN, UK

[2]Department of Biomedical Sciences and Cornell Stem Cell Program, Cornell University, Ithaca, NY, USA

[3]Institute of Clinical Sciences, Imperial College London, Hammersmith Hospital, London W12 0NN, UK

Address for correspondence: David Carling, MRC London Institute of Medical Sciences, Imperial College London, Hammersmith Hospital, London W12 0NN, UK

Email: dcarling@imperial.ac.uk

ABSTRACT

New targets are required for treating prostate cancer, particularly castrate-resistant disease. Previous studies reported that calcium/calmodulin-dependent protein kinase kinase 2 (CAMKK2) expression is increased in human prostate cancer. Here we show that Camkk2 deletion or pharmacological inhibition protects against prostate cancer development in a pre-clinical mouse model that lacks expression of prostate-specific phosphatase and tensin homologue (Pten). In contrast, deletion of AMP-activated protein kinase (Ampk) β1 resulted in earlier onset of adenocarcinoma development. These findings suggest for the first time that Camkk2 and Ampk have opposing effects in prostate cancer progression. Loss of CAMKK2 *in vivo* or in human prostate cancer cells reduced the expression of two key lipogenic enzymes, acetyl-CoA carboxylase and fatty acid synthase. This reduction was mediated via a post-transcriptional mechanism, potentially involving a decrease in protein translation. Moreover, either deletion of CAMKK2 or activation of AMPK reduced cell growth in human prostate cancer cells by inhibiting *de novo* lipogenesis. Activation of AMPK in a panel of human prostate cancer cells inhibited cell proliferation, migration, and invasion as well as androgen-receptor signalling. These findings demonstrate that CAMKK2 and AMPK have opposing effects on lipogenesis, providing a potential mechanism for their contrasting effects on prostate cancer progression *in vivo*. They also suggest that inhibition of CAMKK2 combined with activation of AMPK would offer an efficacious therapeutic strategy in treatment of prostate cancer.

SIGNIFICANCE

Findings show that CAMKK2 and its downstream target AMPK have opposing effects on prostate cancer development and raise the possibility of a new combined therapeutic approach that inhibits CAMKK2 and activates AMPK.

INTRODUCTION

Prostate cancer is the most common cancer in men in the UK and USA, and accounts for almost 20% of all new cancer cases in men in the USA (1). Prostate cancer development is thought to proceed through a series of defined stages, including prostatic intraepithelial neoplasia (PIN), adenocarcinoma and metastatic cancer (2). Standard therapies include androgen ablation therapy and although 80% of patients initially respond favourably most relapse within 1-2 years developing castrate-resistant disease (3). Given the high prevalence and mortality rates associated with prostate cancer, novel drug targets are needed. Two previous studies (4, 5) reported that CAMKK2 gene expression is up-regulated at all stages of human prostate cancer, with evidence that gene expression positively correlates with grade. Both studies provided convincing evidence that the CAMKK2 gene is androgen responsive in human prostate cancer cell lines, providing a potential direct molecular mechanism for up-regulation of CAMKK2 in prostate cancer. Inhibition of CAMKK2 was shown to block androgen stimulated growth, migration and invasion *in vitro* (4, 5), and CAMKK2 inhibition reduced tumour growth in a prostate cancer xenograft model (5). CAMKK2 is one of two upstream kinases (the other being LKB1) that phosphorylates AMPK on threonine 172 (T172) within the α subunit, leading to its activation (6, 7). AMPK is a key regulator of energy homeostasis in eukaryotic cells and activation of AMPK leads to inhibition of protein and lipid synthesis, inhibiting cell growth, and so supporting the hypothesis that AMPK acts as a tumour suppressor (8-12). However, there is also evidence that suggests that under certain circumstances AMPK might help cancer cells survive under adverse nutritional conditions and so support tumour growth (13-17). At the present time, the role of AMPK in prostate cancer remains unclear, and whether AMPK is involved in mediating the downstream effects of CAMKK2 signalling in prostate cancer remains enigmatic.

Here, we use a mouse model of prostate cancer in which the tumour suppressor, phosphatase and tensin homologue (Pten), is deleted specifically in prostate epithelial cells (18) in order to investigate the effect of Camkk2 and Ampk in disease progression *in vivo*. This model accurately recapitulates the different stages seen in the human disease albeit on a more rapid time scale making it an excellent model for the human disease. Consistent with the findings from human prostate cancer, Camkk2 expression is significantly increased in mouse prostate following deletion of *Pten*. We show that CAMKK2 is required for driving protein expression of lipogenic enzymes, leading to increased *de novo* lipogenesis in prostate cancer cells. Conversely, AMPK activation inhibits *de novo* lipogenesis. Genetic deletion of *Camkk2 in vivo* slows prostate cancer development, whereas deletion of *Prkab1* (the gene encoding Ampkβ1) leads to earlier onset of adenocarcinoma. Our findings suggest that CAMKK2 and

AMPK have opposing effects on prostate cancer progression, mediated at least in part by their antagonistic effects on *de novo* lipogenesis.

METHODS

Animal models

All *in vivo* studies were performed in accordance with the United Kingdom Animals (Scientific Procedures) Act (1986) and approved by the Animal Welfare and Ethical Review Board at Imperial College London. All experimental animals were maintained on a C57BL/6J genetic background and fed a chow-standard breeding diet number 3 (Special Diets Services). Mice with prostate-specific deletion of Pten were generated by crossing female *Pten*$^{fl/fl}$ mice (stock number 006440, Jackson Laboratories, Maine USA) with male mice expressing cre-recombinase under the control of a modified rat probasin promoter (*Pbsn-Cre4;* stock number 026662, Jackson Laboratories, Maine USA). Mice with a global deletion of *Camkk2* (deletion of exon 5) were as described previously(19). *Prkab1* floxed mice were generated by crossing Prkab1$^{tm1a(KOMP)Wtsi}$ ("knockout first" mice generated by the trans-NIH Knock-Out Mouse Project (KOMP) and obtained from the KOMP Repository (www.komp.org) with mice expressing Flp-recombinase (stock number 003946, Jackson Laboratories, Maine USA). To generate mice with global deletion of *Camkk2* and prostate-specific deletion of *Pten*, female *Pten*$^{fl/fl}$;*Camkk2*$^{-/-}$ mice were crossed with male *Pbsn-cre4*$^{+}$*; Pten*$^{fl/}$*; Camkk*$^{-/}$ transgenic mice. To generate prostate-specific deletion of *Pten* and *Prkab1,* female *Pten*$^{fl/fl}$*; Prkab1*$^{fl/fl}$ mice were crossed with male *Pbsn-cre4*$^{+}$*; Pten*$^{fl/}$*;Prkab1*$^{fl/}$ transgenic mice.

Histology

Prostates were fixed in 4% paraformaldehyde overnight, wax embedded in paraffin and sectioned to a thickness of 4 microns. Sections were stained with haematoxylin and eosin (H&E) and assessed for disease grading. For Ki-67 and cleaved-caspase3 staining, sections were deparaffinised and rehydrated using Acquaclear, 100% then 70% ethanol and boiled in sodium citrate antigen retrieval solution for 5 minutes in a pressure cooker. Sections were incubated with 0.3% H_2O_2 to block endogenous peroxidase activity, washed with phosphate-buffered saline (PBS) and blocked for 1 hour with 10% normal goat serum in PBS at room temperature. Sections were incubated overnight at 4^{o}C with primary antibody (rabbit anti-Ki-67; Abcam16667 or rabbit cleaved-caspase3; CST#9661 both at a 1:250 dilution). Sections were washed with PBS-tween (0.1%) and incubated with biotinylated goat secondary antibody for 1 hour at room temperature. Sections were then washed with PBS-tween (0.1%) and incubated for 30 minutes with avidin-biotin complex (VECTASTAIN Elite ABC Kit (Vector Laboratories)) according to manufacturer's instructions. Sections were washed with PBS and stained using the DAB Substrate Kit (Vector Laboratories) according to manufacturer's instructions before counterstaining with Gill's haematoxylin (Sigma). Sections were then dehydrated and mounted using DPX mountant (Sigma).

In vivo studies with STO-609

Osmotic minipumps (Models 2004/2006, Alzet Osmotic Pumps, Cupertino, USA) were filled with varying concentrations (6, 15 and 30 mg/ml) of STO-609 (Enzo Life Sciences) in 200 mM NaOH. Addition of STO-609 lowered the pH of the solution to approximately pH 12.8, making it compatible with the minipump specifications. As a vehicle control, 200 mM NaOH was adjusted to pH 12.8 by the addition of HCl. Minipumps were primed at least 48 h before surgery and submersed in PBS at 37^{o}C for several hours to allow the pump to begin operating before implantation. C57BL/6J male mice were anesthetised with isoflurane (Abbott), the interscapular region shaved, and an osmotic minipump inserted subcutaneously. Pump model 2004 (flow rate of 0.25 µl/h; 4 week duration) was used for the initial dosing studies in wild-type mice. 2 weeks after surgery, blood samples were collected into heparinised microvettes (Sarstedt), and the resulting plasma fraction stored at -80^{o}C before analysis for STO-609 levels. After 4 weeks, liver and prostate tissue was collected. Plasma and tissue STO-609 accumulation was analysed by mass spectrometry as described previously by PK/Bioanalytics Core Facility, Cancer Research UK Cambridge Institute, UK. For the intervention studies in *Pten* null mice, pump model 2006 (flow rate of 0.15 µl/h; 6 week duration) was used. Pumps were filled with vehicle (200 mM NaOH, pH adjusted to 12.8) or 30 mg/ml STO-609 in 200 mM NaOH, and implanted into male mice, aged 13 weeks. Six weeks after implantation, animals were sacrificed and prostates removed for subsequent analysis.

Tissue homogenisation

Immediately following dissection, tissues were snap frozen in liquid nitrogen. Frozen tissue was homogenised using an Ultra-Turrax homogeniser in 10x (w/v) ice cold homogenisation buffer containing 50 mM Tris, 50 mM NaF, 5 mM Napyrophosphate, 1 mM EDTA, 0.25 M mannitol, 1 mM dithiothreitol, 157 µg/ml benzamidine, 4 µg/ml trypsin inhibitor and 0.1 mM phenylmethylsulphonyl fluoride. Homogenates were centrifuged at 13,000 x g for 15 minutes to remove insoluble material. Protein content of the soluble fraction was quantified using a BCA assay kit (ThermoScientific).

Western blotting

Proteins were resolved by SDS-PAGE (Novex bis-tris 4-12% gradient gels) and transferred to polyvinylidene difluoride membrane. Primary antibodies were used at a 1/1000 dilution. The following antibodies were from Cell Signalling: rabbit anti-AMPKα1 (#2795), rabbit anti-AMPKα2 (#2757), mouse anti-AMPKα1/2 (#2793), rabbit anti-AMPKβ1/2 (#4150), rabbit anti-ACC (#3676), rabbit anti-pACC (#3661), rabbit anti-AMPKγ1 (#4187), rabbit anti-pThr^{172} (#2535) and rabbit anti-Histone H3 (#4499). Mouse anti-β-actin was from Sigma–Aldrich (A3853). Rabbit anti-AR was from Millipore (06-680). Mouse anti-FASN was from BD laboratories (610963).

Rabbit anti-CAMKK2 was from Atlas and mouse monoclonal anti-CAMKK2 antibody was a generous gift from Prof. Grahame Hardie (Dundee University). Primary antibodies were detected using LI-COR IRDye® Infrared Dye secondary antibodies and visualised using an Odyssey Infrared Imager (LI-COR Biotechnology). Quantification of results was performed using Odyssey software and expressed as a ratio of the signal relative to the signal obtained using an appropriate loading control antibody (either β-actin or tubulin), unless otherwise stated. For AMPK and ACC phosphorylation, blots were quantified relative to total AMPKα or total ACC expression. For capillary western blotting, cell lysates were diluted in HEPES lysis buffer to 0.4 mg/ml. Samples were prepared and analysed according to the manufacturer's instructions (Protein Simple).

Proteomic studies using mass spectrometry

Protein lysates from the anterior lobes of mouse prostate were subjected to overnight digestion with trypsin. Total protein digest was applied to a Thermo Scientific LTQ Orbitrap XL hybrid FTMS (Fourier Transform Mass Spectrometer) operating in positive polarity. Raw data files were analysed using MaxQuant software (www.maxquant.org), and data were searched against the Uniprot mouse database (up-to-date at the time of analysis). In each case, lysates from 3 independent animals, aged 17 weeks, were analysed in duplicate. Proteins with a fold change >2 and $P<0.05$ were determined to be significantly changed between genotypes.

Cell culture

All prostate cancer cell lines (LNCaP, PC3, DU145 and 22Rv1) were obtained from ATCC in 2012. Androgen-responsiveness of LNCaP cells was confirmed. No further authentication was performed. Cells were cultured in RPMI 1640 medium, GlutaMAX (Gibco-61870) supplemented with 10% fetal bovine serum (Sigma-Aldrich), 100 U/ml penicillin, and 100 µg/ml streptomycin. All cells were maintained at 37°C and 5% CO_2 and tested for Mycoplasma using MycoAlert (most recently in May 2018; all cell lines tested were negative). For all studies, passage number was kept below 25. In some cases, cells were treated with 991 (a kind gift from Dr. Jon Read, AstraZeneca, Cambridge) or mibolerone (PerkinElmer). Specific conditions and concentrations are indicated in individual Figure Legends. Cells were serum starved at least 4 h before treatment. Before lysis, cells were washed rapidly three times with ice-cold PBS before the addition of lysis buffer [50 mM (4-(2-hydroxyethyl)-1-piperazineethanesulfonic acid), pH 7.4, 50 mM sodium fluoride, 5 mM sodium pyrophosphate, 1 mM ethylenediaminetetraacetic acid, 10% (v/v) glycerol, 1% (v/v) Triton X-100, 1 mM dithiothreitol, 0.1 mM phenylmethylsulfonyl fluoride, 4 µg/ml trypsin inhibitor and 0.1 mM benzamidine]. Cell lysates were centrifuged at 13000 x g for 15 minutes to remove insoluble material. Protein concentration in the supernatant fraction was

determined by the Bradford Protein Assay using bovine serum albumin (BSA) standards (Bio-Rad, Hertfordshire, UK), according to the manufacturer's protocol.

For investigating the effects of androgen on androgen-responsive LNCap cells, 'starvation media' was used consisting of phenol red-free RPMI supplemented with 5% charcoal-stripped FBS (First Link UK), 100 U/ml penicillin, and 100 µg/ml streptomycin. For culturing cells in the presence of palmitate-bovine serum albumin (BSA) complex, palmitic acid (Sigma) was complexed to fatty acid–free BSA (Roche). Briefly, 40 volumes of a 4% BSA solution in starvation media were added to 1 volume of 50 mM palmitic acid in ethanol and incubated at 37°C for 4 hours, to obtain a 1 mM stock solution of BSA-complexed palmitate. As a control, 4% fatty acid-free BSA was used in place of the BSA-complexed palmitate.

Cytosolic/nuclear fractionation

Cells were lysed in buffer A (40 mM (4-(2-hydroxyethyl)-1-piperazineethanesulfonic acid), pH 7.4, 150 ml NaCl, 2 mM EDTA, 0.4% glycerol, 10 mM β-glycerophosphate and 0.4% Triton). Samples were centrifuged at 1270 x g for 10 minutes at 4°C. The cytosolic supernatant fraction was collected on ice. The nuclear pellet was resuspended in buffer A and centrifugation repeated. The supernatant was discarded and the pellet was resuspended in nuclear extraction buffer (10 mM Tris-HCl pH 7.4, 1.5 mM NaCl, 1% Triton X-100). Nuclear samples were briefly sonicated. Nuclear and cytosolic samples were centrifuged at 13000 x g for 10 minutes at 4°C. Supernatant fractions were collected and analysed, or stored at -80°C for further use.

CAMKK2 deletion via CRISPR

LNCaP cells were transfected with plasmids containing Cas9 linked to green fluorescent protein (GFP) via a self-cleaving peptide and guide sequences targeting the first exon of CAMKK2 (GCTAGAGACACATGATGACA, GCAGGGCCTCACAGGGCTTC, GGTGGATGCTCAAGGATGAG, GGGCATGGAGTCCTTCATTG, AGCACAGCCCGGCTCACACT; Horizon Discovery, Cambridge, U.K.). At 24 h post-transfection, cells were sorted based on GFP expression and individual colonies were analysed by Western blotting to determine CAMKK2 protein expression. Cells lacking CAMKK2 expression were maintained for subsequent studies and used within 10 passages from isolation.

RNA isolation and quantitative PCR

RNA was isolated from human prostate cancer cells and mouse prostates by homogenization in Trizol reagent (Invitrogen) according to the manufacturer's instructions, followed by purification on an RNeasy column (Qiagen). First strand cDNA synthesis using Superscript II (Invitrogen) according to the manufacturer's instructions and quantitative PCR was done with SensiMix Plus SYBR kit (Quantace) using the primer detailed in Supplementary Table 1. In mouse prostate

tissue, mRNA expression was normalised to an averaged housekeeper gene set (*Rps14, Hmbs, Ppia*), whereas in human cell lines, expression was normalised to *36B4*.

AMPK assay

AMPK complexes were immunoprecipitated from prostate cancer cell lysates using a rabbit pan-AMPKβ antibody bound to protein A-Sepharose (Woods et al., 1996) and activity present in the immune complexes was determined by phosphorylation of the SAMS peptide, as previously described (Davies et al., 1989).

Proliferation assay

Depending on cell line, 5000-7000 cells were seeded per well in a 96-well plate and left to adhere for 24 h. Cell media was changed and fresh media added containing 50 μM BrdU (Sigma) and 991 (at the concentration indicated in the legend) or vehicle control (5% DMSO). After 16 h, cells were washed twice with PBS and fixed using 4% (w/v) paraformaldehyde in PBS. Permeabilisation of the membrane was achieved by incubation with 0.2% Triton X-100 in PBS for 10 minutes, cells were then washed with PBS and blocked for 1 h with blocking solution (1% BSA/0.2% fish gelatin in PBS). Cells were incubated for 30 minutes with a 1/2000 dilution of anti-BrdU antibody (BD Pharmingen 555627), 20 U/μl DNase1 (Sigma) and 1mM $MgCl_2$ in blocking solution. Cells were washed 3 times with PBS and then incubated with secondary antibody (goat anti-mouse, Alexa Fluor® 488 conjugate) at a 1/500 dilution in blocking solution for 30 minutes. Cells were then washed a further 3 times and counter stained with 4',6-diamidino-2-phenylindole (DAPI; 1 μg/ml) for 30 minutes. Image acquisition was achieved on the INCell Analyser 1000 Cell Imaging System (GE Healthcare, Life Sciences) using the 20x/0.45 Plan Fluor objective. Image acquisition was automated and 16 frames were taken per well. Images were analysed using the INCell 1000 Image Analysis Software.

Cell cycle analysis

Cells were treated with DMSO or 991 for 16 h, trypsinised and counted using the Guava ViaCount assay. $1x10^6$ cells in 0.5 ml were then added to 4.5 ml of ice cold 70% ethanol and left to fix overnight at 4^oC. Cells were washed twice with PBS and re-dissolved in 300 μl of propidium iodide (PI)/RNase Staining Solution (CST) for 30 minutes at room temperature in the dark before being analysed on BD LSR II Flow Cytometer (BD Biosciences).

Cell viability assay

Cells were trypsinised and 10 μl of cell suspension was mixed with 190 μl ViaCount assay reagent (Merck) and incubated for 5 minutes at room temperature. Viability data were acquired on a Guava easyCyte instrument (Merck) using GuavaSoft 3.1.1 software.

Migration assay

Cells were plated in a 6-well plate and grown until confluent. Using a pipette tip, a scratch was created in the confluent monolayer of cells. The cells were then washed twice with serum-free media and fresh media containing 991 (at the concentration indicated in the legend) or vehicle control (5% DMSO) was added. Six regions-of-interest were picked per well and images were taken every 30 minutes using an UltraVIEW Live Cell Imaging System (x20 objective) (PerkinElmer). Cells were maintained at 37°C and 5% CO_2 for the duration of image acquisition. Quantification of the datasets generated was performed using a programme developed in collaboration with the LMS MRC microscopy facility. Briefly, the software developed calculated the area covered by cells based on a texture algorithm. As cells migrated to fill the scratch, the textured area increased and this was used as a read-out of cell migration.

Invasion assay

Invasion assays were performed on the xCELLigence RTCA DP (ACEA Biosciences, Inc) and data analysed using the RTCA 2.0 Software. CIM-plates (Cambridge BioScience, UK) were coated with Matrigel (BD Bioscience) using a 1/40 dilution (1 Matrigel:40 SFM) and performed according to manufacturer's instructions. 40k cells were plated and invaded down a serum gradient of 0-10%. Assays were performed over 48 h with readings taken every 15 minutes.

Lipogenesis assay

Wild-type and CAMKK2 KO LNCaP cells were incubated in serum-free RPMI media in the presence and absence of 1 nM mibolerone for 24 h prior to labelling. Media was then changed to media containing 2 mM sodium acetate and 5 µCi/ml [^{3}H] sodium acetate (Perkin Elmer) in the presence and absence of mibolerone (1 nM) and/or 991 (10 µM) and incubated for 24 h. Cells were washed gently with PBS and harvested in PBS containing 2 mM EDTA. Cell pellets were then re-suspended in PBS and split into two for lipid analysis and protein concentration determination. Lipid was extracted from cell pellets using the Folch method (Folch, 1957) and the lipid containing fraction evaporated to dryness before determining ^{3}H incorporation by scintillation counting.

Cell growth assay

For palmitic acid rescue experiments cells were seeded in either a 24- or 96- well plate at a density of $1.5x10^4$ (24-well) or $3.5x10^3$ (96-well) cells per well, and left to adhere overnight before treatment. 96-well plates were coated with poly lysine before seeding. After 3 days, cell growth was assayed using alamarBlue reagent (ThermoFisher), according to manufacturer's instructions. Briefly, alamarBlue reagent was added as 10% of sample volume and incubated for

2 hours at 37^{o}C before fluorescence was read. No difference in fluorescence intensity was seen between wild-type and CAMKK2 KO LNCaP cells before treatment.

Statistical analysis

Unless otherwise stated, data are expressed as mean ± SEM. Graphpad Prism software was used for graphing and statistical analysis. For comparison between two groups, datasets were analysed using Student's t-test, with a statistically significant difference defined as $P<0.05$. To compare three or more data sets, a one-way analysis of variance (one-way-ANOVA) was used, followed by Bonferroni's range test to measure significance between means. Multiple comparisons were compared using two-way ANOVA with post-hoc Tukey's test.

RESULTS

Camkk2 expression regulates prostate cancer progression in vivo

To investigate the role of Camkk2 in prostate cancer we made use of the previously characterised *Pten* mouse model of prostate cancer (18). In this model, Cre-recombinase is under the control of a modified rat prostate-specific probasin promoter (PB-Cre4) (20) that drives deletion of the floxed *Pten* allele in the epithelial cells of the mouse prostate. *Camkk2* mRNA and protein were significantly increased in the *Pten* knockout (KO) mice (hereafter, referred to as *Pten* mice) compared to wild-type controls (Fig.1A), recapitulating the increase in CAMKK2 expression in human prostate cancer (4, 5). *Pten* mice were crossed with mice with global deletion of *Camkk2* (19) to generate mice lacking both *Pten* and *Camkk2* in the prostate (hereafter, referred to as *Pten;Camkk2*). As anticipated, *Camkk2* gene expression was significantly reduced in the *Pten;Camkk2* mice, with undetectable levels of Camkk2 mRNA and protein in the prostate (Figs.1A,B). Prostate cancer development was monitored in the *Pten* and *Pten;Camkk2* mice at 12, 17 and 26 weeks of age. Prostate tissue weight was significantly decreased in the *Pten;Camkk2* mice compared to the *Pten* mice at all three time points (Fig.1C and Supplementary Fig.S1A), indicating that *Camkk2* deletion was reducing disease progression. To confirm this, histopathological analysis was performed on haematoxylin and eosin (H&E) stained prostate sections from 26 week old animals. Prostates from the *Pten;Camkk2* mice were found to display significantly less grade 4 prostatic intraepithelial neoplasia (PIN) relative to the *Pten* mice (Fig.1D). This lesion is the most severe PIN grade preceding invasive adenocarcinoma development. Representative images of prostate tissue sections highlighting the different grades are shown in Supplementary Fig.S1B. To investigate whether *Camkk2* deletion affected cell proliferation, prostate tissue sections from 26 week old animals were stained for Ki-67, a marker of cell proliferation. Ki-67 staining was significantly reduced in prostate from the *Pten;Camkk2* mice compared to *Pten* mice (Fig.1E and Supplementary Fig.S2A). We also noted an increase in the number of apoptotic cells, as determined by increased reactivity for cleaved-caspase 3 (Supplementary Fig.S2B), together with increased desmoplasia. These results suggest Camkk2 is required to support increased cellular proliferation and cell survival in *Pten* prostate tissue. Prostate sections stained with Masson's trichrome revealed significantly less collagen deposition in *Pten;Camkk* mice compared to *Pten* mice (Supplementary Fig.S2C).

In the studies described above, mice were studied up to 26 weeks of age. At this time point, we observed grade 4 PIN in 100% of the *Pten* mice (10/10) compared to 12.5% of the *Pten;Camkk* mice (1/8). However, we did not detect adenocarcinoma at this time point. We therefore bred another cohort of animals and maintained these for 40 weeks. During this time, 3 out of the 9 *Pten* mice had to be culled prematurely, as they displayed obvious signs of ill health. In contrast, none of the *Pten;Camkk2* mice showed any signs of adverse health. At 40

weeks, 67% (4/6) of the remaining *Pten* mice had adenocarcinoma, compared to none (0/5) of the *Pten;Camkk2* mice (Fig.1F). Although these results did not reach statistical significance (Fisher's exact test gave two-sided *P* value = 0.06), the findings suggest a strong trend for protection against adenocarcinoma at 40 weeks of age.

Camkk2 inhibition is a promising therapeutic strategy to treat prostate cancer

To investigate whether CAMKK2 inhibition has a beneficial effect following disease onset, *Pten* mice were treated with STO-609, an inhibitor of CAMKK2 (21). We used osmotic minipumps to administer STO-609 *in vivo*, and our preliminary studies showed that steady-state plasma levels of STO-609 reached a plateau of approximately 1 μM with concentrations ≥15 mg/ml in the minipump reservoir (Fig.2A). This steady-state plasma concentration is similar to the peak plasma concentration measured in a previous study following dosing via either intravenous or intraperitoneal injection (5). We also confirmed STO-609 accumulation in both prostate and liver tissue (Fig.2B). *Pten* mice were treated with STO-609 (15 mg/ml) or vehicle for 6 weeks from 13 weeks of age. Prostates from STO-609 treated mice were significantly smaller than vehicle treated controls, with an average reduction in weight of over 30% (Figs.2C,D). Immunohistochemical analysis of the anterior lobes revealed that STO-609 treatment reduced progression from PIN3 to PIN4 (Fig.2E). These results support the hypothesis that CAMKK2 inhibition can be used as a therapeutic intervention to slow the development of prostate cancer.

***Prkab1* deletion leads to early onset of adenocarcinoma**

Since CAMKK2 is upstream of AMPK, previous studies investigating the role of CAMKK2 in prostate cancer have attempted to link its role to signalling through AMPK (4, 5). However, the precise molecular mechanism by which AMPK activation might lead to an increase in prostate cancer cell growth remains unclear. Ampk expression, and phosphorylation of T172, are markedly increased in prostate tissue from *Pten* mice compared to wild-type controls (Figs.3A,B). These increases were significantly reduced in the *Pten;Camkk2* tissue (Fig.3A). Deletion of *Pten* caused a greater increase in Ampkβ1 expression relative to Ampkβ2 (Fig. 3A). A previous study reported that AMPKβ1 was required for prostate cancer cell survival (22). To investigate further the role of AMPK, and in particular AMPKβ1, in prostate cancer, we generated prostate-specific *Pten;Prkab1 (*encoding *Ampkβ1)* null mice by crossing *Pten* and *Prkab1* floxed mice with mice expressing PB-Cre4 (hereafter referred to as *Pten;Prkab1*). We were unable to use the global *Prkab1* KO as these mice displayed an adverse phenotype including haemolytic anaemia and splenomegaly (Supplementary Figs.S3A-C) that would confound the study. Although this phenotype was not reported previously for the global *Prkab1*

KO (23), a similar phenotype has been reported for both the *Prkaa1* (24) and *Prkag1* (25) global KO mouse models.

Expression of Ampk subunits (α1, β1 and γ1), as well as T172 phosphorylation, was reduced in the *Pten;Prkab1* mice relative to *Pten* mice prostate tissue (Fig.3B). Note that in this model there is still Ampk expression in prostate from the Prkab1 deleted mice since Ampkβ2 expression is not affected, and because Ampkβ1 is expressed in non-epithelial cells present within the tissue, which is not affected by the PB-Cre4 mediated deletion. There was no significant difference in prostate weight between *Pten* and *Pten;Prkab1* mice (Fig.3C). However, histopathological analysis of serial H&E stained sections revealed that by 26 weeks of age nearly 60% (4/7) of prostates from *Pten;Prkab1* mice had invasive adenocarcinoma, whereas none of the prostates from *Pten* mice had developed adenocarcinoma (Fig.3D). Consistent with Ampkβ1 acting as a tumour suppressor, prostates from *Pten;Prkab1* mice were found to have significantly increased Ki-67 staining, indicative of increased cell proliferation (Figs.3E,F). These results suggest for the first time that Ampkβ1 plays a protective role in prostate cancer progression, implying that Ampk and Camkk2 have opposing roles in prostate cancer.

CAMKK2 increases fatty acid synthesis through upregulation of lipogenic enzyme protein expression

Our findings support the hypothesis that increased CAMKK2 expression drives prostate cancer progression. In order to gain insight into the mechanisms underlying this effect we carried out an unbiased proteomic screen on prostate tissue from *Pten* and *Pten;Camkk2* mice aged 17 weeks. Fifty-one proteins were found to be significantly down-regulated, and 23 significantly up-regulated, (>2-fold change, $P<0.05$) in the *Pten;Camkk2* mice relative to *Pten* mice (Table 1). Fatty acid synthase (Fasn) was one of the significantly down-regulated proteins in the *Pten;Camkk2* mice. Previous studies have shown that increased *de novo* liopgenesis acts as a key driver of prostate cancer (26, 27), and that increased expression of FASN is a prominent feature in human cancers (28). In order to validate the change in Fasn, we measured its expression in prostate tissue from wild-type, *Camkk2*, *Pten* and *Pten;Camkk2* mice by Western blotting (Fig.4A). Pten deletion caused a 5-fold increase in Fasn expression relative to wild-type mice, and deletion of Camkk2 significantly decreased expression in both Pten expressing and Pten null prostate tissue (Fig.4A). In human tumours acetyl-CoA carboxylase 1 (ACC1) expression is increased in conjunction with FASN to upregulate lipid synthesis. Acc1 was absent from our data-set, but Western blotting showed that Acc1 expression followed a similar pattern to Fasn (Fig.4A).

To determine whether the changes in protein expression were correlated to gene expression, mRNA levels were determined. As shown in Fig.4B, loss of Pten caused a

significant increase in the expression of both Acc1 and Fasn mRNA. However, this increase was not affected by deletion of Camkk2 (Fig.4B), suggesting that the changes in protein expression are mediated by post-transcriptional mechanisms. We noted that 5 of the most highly down-regulated proteins in the *Pten;Camkk2* mice corresponded to eukaryotic initiation factors (Eif3a, Eif3c, Eif3e, Eif4a1, Eif4a2; see Table 1) and gene set enrichment analysis revealed eukaryotic protein translation as the most significantly altered pathway between *Pten* and *Pten;Camkk2* mice. These changes suggest that Camkk2 may play a role in regulating protein translation, and that this could account for the reduced expression of Fasn and Acc1 in mice lacking Camkk2.

In order to investigate functional significance, we deleted CAMKK2 from LNCaP cells, an androgen-sensitive human prostate cancer cell line, using the CRISPR/Cas 9 system. Similar to previous studies (4, 5), we observed an increase in CAMKK2 protein in wild-type LNCaP cells treated with a synthetic androgen, mibolerone, whereas CAMKK2 was not detectable in the CAMKK2 KO cells (Fig.4C). Mibolerone increased protein levels of both ACC1 and FASN, but to a lesser extent in cells lacking CAMKK2 (Fig.4D). Activation of AMPK by 991, a direct activator of AMPK, also reduced ACC1 and FASN protein expression in mibolerone treated cells (Fig.4C). In both cases, the effects on ACC1 expression tended to be greater than on FASN. In parallel with the decreased expression of ACC1 and FASN, lipogenesis was reduced in the CAMKK2 KO cells relative to the wild-type cells in all conditions tested (Fig.4D). Androgen treatment caused a significant increase in lipogenesis in wild-type cells (1.8-fold) and, to a lower extent, in CAMKK2 KO cells (1.4-fold). The effect of CAMKK2 deletion on both lipogenic enzyme expression and lipogenesis was more pronounced in androgen stimulated cells. Under these conditions, CAMKK2 expression is increased in wild-type cells. Consistent with a previous study (29), activation of AMPK in LNCaP cells inhibited lipogenesis and this effect was seen in both wild-type and CAMKK2 KO cells, in the absence or presence of androgen (Fig.4D). CAMKK2 deletion or activation of AMPK reduced cell growth of the LNCaP cells by a similar degree, and in both cases this effect was rescued by addition of exogenous palmitic acid to the cell media (Fig.4E). Treatment of the CAMKK2 KO cells with 991 caused a further small reduction in cell growth, which also was reversed by addition of palmitic acid (Fig.4E). These results suggest strongly that the reduction in cell growth caused by deletion of CAMKK2, or by activation of AMPK, is mediated by a reduction in *de novo* lipogenesis.

AMPK activation reduces prostate cancer cell proliferation, migration and invasion

Our results support the hypothesis that activation of AMPK would be beneficial in treating prostate cancer. Previous studies investigating the role of AMPK in prostate cancer used indirect AMPK activators such as metformin and 5-aminoimidazole-4-carboxamide riboside (AICAR), which are known to have AMPK-independent effects (13, 30). In order to

circumvent these issues, we used the highly selective and direct AMPK activator, 991 (31), to activate AMPK and assess its effect on proliferation, migration, and invasion in a panel of human prostate cancer cell lines. The prostate cancer cell line panel included cell lines with a range of driver mutations and androgen receptor (AR) responsiveness, and displaying different migratory and invasive capacities, allowing us to determine the efficacy of AMPK activation in different genetic contexts. In all cell lines used, 991 caused a dose-dependent increase in AMPK activity and increased phosphorylation of T172 and ACC1 (Figs.5A,B and Supplementary Fig.S4). AMPK activation was found to significantly inhibit cell proliferation in all prostate cancer cell lines (Fig.5C), leading to a 30-40% reduction in proliferation over 16 h. Flow cytometry analysis revealed a greater population of cells in G1 phase after AMPK activation, implying AMPK activation was inhibiting S phase entry (Fig.5D). Treatment with 991 had no effect on cell viability (Fig.5E). AMPK activation led to a significant decrease in cell migration. The results for 22Rv1 cells, which showed the highest level of migration, are shown in Fig.5F. Similar results were observed in DU145 and PC3 cells (Supplementary Fig.S5); LNCaP cells did not migrate appreciably under these conditions. Finally, AMPK activation was found to drastically reduce cell invasion in 22Rv1 cells (Fig.5G). Taken together these results indicate that AMPK activation lowers prostate cancer cell tumourigenicity.

AMPK activation inhibits androgen receptor activity

Previous studies reported that AMPK activation inhibits AR function in prostate cancer cells (32). On the other hand, AR increases CAMKK2 expression, leading to increased AMPK activity (4, 5). These findings suggest the possibility of a negative-feedback loop involving AR-mediated induction of CAMKK2 expression with the subsequent activation AMPK leading to inhibition of AR function (32). Since we found that CAMKK2 and AMPK have opposing effects in prostate cancer, we decided to re-visit their effects on AR signalling in AR-responsive human LNCaP cells. Consistent with previous studies (4, 5), we found that CAMKK2 expression is significantly increased in wild-type LNCaP cells following treatment with androgen (Fig.4D). In wild-type cells, phosphorylation of AMPK and ACC1 were increased following androgen stimulation and these were markedly reduced in CAMKK2 KO cells (Fig. 6A). These results suggest that AMPK activation downstream of AR signalling is dependent on CAMKK2.

Translocation of AR to the nucleus following ligand binding is a key step in AR regulation of transcription (33). In addition to a significant increase in AR expression, mibolerone treatment caused an increase in AR nuclear localisation (Fig.6B). Activation of AMPK resulted in decreased AR expression in both basal and mibolerone treated cells. Strikingly, AMPK activation almost completely blocked AR expression in the nucleus in the presence of mibolerone (Fig.6B). Consistent with the reduction of AR protein and nuclear exclusion, AMPK activation was found to drastically reduce expression of AR-induced genes (Fig.6C), including

CAMKK2. These results suggest that AMPK activation antagonises AR signalling in human prostate cancer cells, and so support our findings that they have opposing effects on prostate cancer development in vivo in a mouse model (Fig.6D).

DISCUSSION

In castration-resistant patients, AR signaling is often reactivated in the absence of androgens (2, 3, 34, 35). Targeting pathways downstream of the AR therefore provides an attractive additional strategy to combat advanced prostate cancer. Here we show for the first time that genetic deletion or pharmacological inhibition of CAMKK2 reduces prostate cancer progression *in vivo* in a pre-clinical mouse model. In contrast, inhibition of AMPK, via genetic deletion of AMPKβ1, increases disease progression. Supporting the *in vivo* studies, we show that CAMKK2 and AMPK have opposing effects on *de novo* lipogenesis and cell growth in human prostate cancer cells. Taken together, our results raise the possibility of a dual combination therapy of CAMKK2 inhibition together with AMPK activation as an efficacious treatment for prostate cancer.

Whilst the evidence supporting a tumour-promoting role for CAMKK2 in prostate cancer is strong, the mechanism by which CAMKK2 exerts its effect remains unclear. CAMKK2 is upstream of AMPK and two previous studies have implicated AMPK downstream of CAMKK2 in promoting prostate cancer cell growth (4, 5). One of these studies reported that AMPK activation partially rescued the growth inhibitory effect of CAMKK2 inhibition in LNCaP cells (5), whilst the other showed that depletion of AMPK decreased LNCaP cell migration (4). Two other studies reported that inhibition of AMPK reduced prostate cancer cell growth *in vitro* (22, 36). Other studies, however, reported that AMPK activation decreases cell growth of LNCaP cells, and this was associated with decreased expression of FASN (29, 37). It is difficult to reconcile these findings, but the differences are likely due in part to the use of non-specific compounds to activate and/or inhibit AMPK (30, 38). These conflicting findings leave unresolved the issue of whether or not CAMKK2 promotes prostate cancer growth via activation of AMPK *in vivo*. We observed a marked increase in expression of Ampk subunits, as well as increased phosphorylation of T172, in the *Pten* mouse model. In human prostate cancer tissues, increased phosphorylation of AMPK T172 (39) and ACC1 (36) has been reported.

In order to gain understanding of the role of AMPK in prostate cancer *in vivo* we investigated the effect of deletion of *Prkab1* in the prostate-specific *Pten* null model. We focused on deletion of *Prkab1* since AMPKβ1 was identified from an siRNA screen as a specific candidate required for prostate cancer cell growth (22). In addition, we found that Ampkβ1 expression, but not Ampkβ2, is increased in prostate tissue following *Pten* deletion, and this increase is reduced by deletion of *Camkk2*. Deletion of *Prkab1* led to an earlier onset of invasive adenocarcinoma in the *Pten* model, combined with significantly increased cell proliferation. These results demonstrate that Ampkβ1 plays a protective role in prostate cancer progression *in vivo*. We would suggest that the increase in AMPK observed in human prostate cancer (36, 39) is part of a protective cellular mechanism.

Acc1 and Fasn expression were markedly reduced in prostate from *Pten;Camkk2* mice compared to *Pten* mice, and a similar effect was seen upon CAMKK2 deletion in human prostate cancer cells. Many cancer cells have increased rates of *de novo* lipogenesis, and this is associated with high levels of ACC1 and FASN expression. Increased *de novo* lipogenesis is now recognized as a common feature of highly proliferating cancer cells (27, 40). The effect of Camkk2 on Acc1 and Fasn expression appears to occur at a post-transcriptional level since there was no effect of Camkk2 deletion on their mRNA levels. At present, we do not know the exact mechanism by which Camkk2 leads to increased Acc1 and Fasn protein expression. However, we did note that several translation initiation factors were amongst the proteins down-regulated in the *Pten;Camkk2* model suggesting that changes in protein translation could be affected. It is now appreciated that the translational landscape is drastically altered in prostate cancer (41), although the regulation and importance of this is only poorly understood. CAMKK2 has been shown to regulate protein synthesis in hepatocellular carcinoma (42) and in neurons (43, 44). In hepatocellular carcinoma, signaling was reported to be via CAMKIV (42), although CAMKI was found to be important for regulating translation initiation in neurons (44). Intriguingly, a recent study reported that CAMKK2 activates Akt in ovarian cancer cells by directly phosphorylating threonine 308 in Akt, and that this activation promoted many of the downstream effects of Akt, including increased protein synthesis (45). It is possible that CAMKK2 plays a wider role in regulating protein synthesis in other types of cancer and/or in other cells types such as neurons.

A key finding from the present study is that deletion of CAMKK2 reduces *de novo* lipogenesis and cell growth in human prostate cancer cells. Interestingly, two recent independent studies (46, 47) show a critical role for increased lipogenesis in prostate cancer progression using the same mouse model as in the current study. The stimulatory role of CAMKK2 on lipogenesis could provide part of the mechanism underlying our finding that Camkk2 and Ampk have opposing effects on prostate cancer progression *in vivo*. AMPK is a well-established negative regulator of lipogenesis, and activation of AMPK has been shown to reduce prostate cancer cell proliferation via inhibition of lipogenesis (29). We show that the reduced cell growth resulting from loss of CAMKK2, or activation of AMPK, is due to decreased lipogenesis, since addition of exogenous palmitic acid rescues this effect. A likely target for both CAMKK2 and AMPK is ACC1. It is well established that AMPK phosphorylates and inhibits ACC1, and we show here that CAMKK2 deletion leads to a reduction in ACC1 expression, in both human and mouse models. In two previous studies (29, 48), it was shown that inhibition of ACC1 using 5-(tetradecyloxy)-2-furoic acid (TOFA) reduced lipogenesis and cell growth in LNCaP cells. In conjunction with the results of our present study, these combined findings suggest that inhibiting lipogenesis through different signaling pathways could provide attractive strategies for treating prostate cancer. Treatment with 991 reduced lipogenesis and cell growth

in CAMKK2 KO cells demonstrating that AMPK is still responsive to activation in the absence of CAMKK2. This is presumably mediated via phosphorylation of AMPK T172 by LKB1 and/or allosteric activation by 991. These findings have significant implications as they suggest that CAMKK2 and AMPK regulate lipogenesis through independent mechanisms.

In Fig. 6D, we propose a model in which CAMKK2 and AMPK have antagonistic effects on *de novo* lipogenesis and prostate cancer progression. Our data shows that CAMKK2 activates AMPK in response to androgen signalling, and AMPK inhibits AR function, forming a negative feedback loop, consistent with a previous study (32). In addition, AMPK has been reported to inhibit the calcium/calmodulin independent activity of CAMKK2 by directly phosphorylating CAMKK2 on T144 (49). At the current time, it is unclear as to how these negative feedback loops function *in vivo*. Both CAMKK2 and AMPK represent attractive druggable targets for which tool compounds are already available. Whilst our findings support a role for AMPKβ1 in slowing prostate cancer progression, they do not rule out the possibility that AMPKβ2-containing complexes could have different effects in prostate cancer. An important consideration in this regard is that AMPKβ1-specific activators have been generated (50). The availability of AMPKβ1-specific activators would avoid any potential complications that might arise with activation of AMPKβ2-complexes. We observed an additive effect of CAMKK2 deletion and AMPK activation in reducing lipogenesis in human prostate cancer cells suggesting that a dual combination therapy of CAMKK2 inhibition and AMPK activation could provide a more efficacious strategy for treatment of prostate cancer.

Disclosure of Potential Conflicts of Interest

The authors declare that there are no potential conflicts of interest.

Acknowledgments

This work was funded by grant MC-A654-5QB10 from the Medical Research Council UK to D. Carling and grants from the US National Institutes of Health (NIH) and National Cancer Institute (NCI) (CA197160), and NYSTEM (C029155) to A,Y. Nikitin. L. Penfold received an Imperial Beit Fellowship from Imperial College London and an MRC PhD studentship from the Medical Research Council UK. We are grateful to the Flow Cytometry, Mass Spectrometry and Proteomics, and Microscopy Facilities at the London Institute of Medical Sciences for their invaluable assistance. We would like to thank Daisy Luff, Lizzie Sandham, Berengere Snyers and Emma Battell for their help with some of the experiments.

REFERENCES

1. Siegel RL, Miller KD, A J. Cancer statistics, 2018. CA: A Cancer Journal for Clinicians. 2018;68:7-30.
2. Abate-Shen C, Shen MM. Mouse models of prostate carcinogenesis. Trends Genet. 2002;18:S1-S5.
3. Yuan X, Cai C, Chen S, Chen S, Yu Z, Balk SP. Androgen receptor functions in castration-resistant prostate cancer and mechanisms of resistance to new agents targeting the androgen axis. Oncogene. 2014;33:2815-25.
4. Frigo DE, Howe MK, Wittmann BM, Brunner AM, Cushman I, Wang Q, et al. CaM kinase kinase beta-mediated activation of the growth regulatory kinase AMPK is required for androgen-dependent migration of prostate cancer cells. Cancer Res. 2011;71(2):528-37.
5. Massie CE, Lynch A, Ramos-Montoya A, Boren J, Stark R, Fazli L, et al. The androgen receptor fuels prostate cancer by regulating central metabolism and biosynthesis. EMBO J. 2011;30:2719-33.
6. Hawley SA, Pan DA, Mustard KJ, Ross L, Bain J, Edelman AM, et al. Calmodulin-dependent protein kinase kinase-beta is an alternative upstream kinase for AMP-activated protein kinase. Cell Metab. 2005;2(1):9-19.
7. Woods A, Dickerson K, Heath R, Hong SP, Momcilovic M, Johnstone SR, et al. Ca2+/calmodulin-dependent protein kinase kinase-beta acts upstream of AMP-activated protein kinase in mammalian cells. Cell Metab. 2005;2(1):21-33.
8. Carling D. AMPK signalling in health and disease. Curr Opin Cell Biol. 2017;45:31-7.
9. Faubert B, Boily G, Izreig S, Griss T, Samborska B, Dong Z, et al. AMPK is a negative regulator of the Warburg effect and suppresses tumor growth in vivo. Cell Metab. 2013;17:113-24.
10. Garcia D, Shaw RJ. AMPK: Mechanisms of Cellular Energy Sensing and Restoration of Metabolic Balance. Mol Cell. 2017;66:789-800.
11. Houde VP, Donzelli S, Sacconi A, Galic S, Hammill JA, Bramson JL, et al. AMPK b1 reduces tumor progression and improves survival in p53 null mice. Mol Oncol. 2017;11:1143-55.
12. Shackelford DB, Abt E, Gerken L, Vasquez DS, Seki A, Leblanc M, et al. LKB1 inactivation dictates therapeutic response of non-small cell lung cancer to the metabolism drug phenformin. Cancer Cell. 2013;23:143-58.
13. Carling D, Thornton C, Woods A, Sanders MJ. AMP-activated protein kinase: new regulation, new roles? Biochem J. 2012;445(1):11-27.
14. Hardie DG. Molecular Pathways: Is AMPK a Friend or a Foe in Cancer? Clin Cancer Res. 2015;21(17):3836-40.
15. Jeon SM, Chandel NS, Hay N. AMPK regulates NADPH homeostasis to promote tumour cell survival during energy stress. Nature. 2012;485:661-5.
16. Jeon SM, Hay N. The double-edged sword of AMPK signalling in cancer and its therapeutic implications. Arch Pharm Res. 2015;38:346-57.
17. Vara-Ciruelos D, Dandapani M, Gray A, Egbani EO, Evans AM, Hardie DG. Genotoxic Damage Activates the AMPK-α1 Isoform in the Nucleus via Ca2+/CaMKK2 Signaling to Enhance Tumor Cell Survival. Mol Cancer Res. 2018;16:345-57.
18. Wang S, Gao J, Lei Q, Rozengurt N, Pritchard C, Jiao J, et al. Prostate-specific deletion of the murine Pten tumor suppressor gene leads to metastatic prostate cancer. Cancer Cell. 2003;4:209-21.
19. Peters M, Mizuno K, Ris L, Angelo M, Godaux E, Giese KP. Loss of Ca2+/calmodulin kinase kinase beta affects the formation of some, but not all, types of hippocampus-dependent long-term memory. J Neurosci. 2003;23(30):9752-60.
20. Wu X, Wu J, Huang J, Powell WC, Zhang J, Matusik RJ, et al. Generation of a prostate epithelial cell-specific Cre transgenic mouse model for tissue-specific gene ablation. Mech Dev. 2001;101:61-9.
21. Tokumitsu H, Inuzuka H, Ishikawa Y, Ikeda M, Saji I, Kobayashi R. STO-609, a specific inhibitor of the Ca(2+)/calmodulin-dependent protein kinase kinase. J Biol Chem. 2002;277(18):15813-8.

22. Ros S, Santos CR, Moco S, Baenke F, Kelly G, Howell M, et al. Functional metabolic screen identifies 6-phosphofructo-2-kinase/fructose-2,6-bisphosphatase 4 as an important regulator of prostate cancer survival. Cancer Discov. 2012;2:328-43.
23. Dzamko N, van Denderen BJ, Hevener AL, Jørgensen SB, Honeyman J, Galic S, et al. AMPK beta1 deletion reduces appetite preventing obesity and hepatic insulin resistance. J Biol Chem. 2010;285:115-22.
24. Foller M, Sopjani M, Koka S, Gu S, Mahmud H, Wang K, et al. Regulation of erythrocyte survival by AMP-activated protein kinase. FASEB J. 2009;23(4):1072-80.
25. Foretz M, Hébrard S, Guihard S, Leclerc J, Do Cruzeiro M, Hamard G, et al. The AMPKg1 subunit plays an essential role in erythrocyte membrane elasticity, and its genetic inactivation induces splenomegaly and anemia. FASEB J. 2011;25:337-47.
26. Ettinger SL, Sobel R, Whitmore TG, Akbari M, Bradley DR, Gleave ME, et al. Dysregulation of sterol response element-binding proteins and downstream effectors in prostate cancer during progression to androgen independence. . Cancer Res. 2004;64:2212-21.
27. Santos CR, Schulze A. Lipid metabolism in cancer. FEBS J. 2012;279:2610-23.
28. Flavin R, Zadra G, Loda M. Metabolic alterations and targeted therapies in prostate cancer. J Pathol. 2011;223:283-94.
29. Zadra G, Photopoulos C, Tyekucheva S, Heidari P, Weng QP, Fedele G, et al. A novel direct activator of AMPK inhibits prostate cancer growth by blocking lipogenesis. EMBO Mol Med. 2014;6:519-38.
30. Foretz M, Hébrard S, Leclerc J, Zarrinpashneh E, Soty M, Mithieux G, et al. Metformin inhibits hepatic gluconeogenesis in mice independently of the LKB1/AMPK pathway via a decrease in hepatic energy state. J Clin Invest. 2010;120:2355-69.
31. Xiao B, Sanders MJ, Carmena D, Bright NJ, Haire LF, Underwood E, et al. Structural basis of AMPK regulation by small molecule activators. Nat Commun. 2013;4:3017.
32. Jurmeister S, Ramos-Montoya A, Neal DE, Fryer LG. Transcriptomic analysis reveals inhibition of androgen receptor activity by AMPK in prostate cancer cells. Oncotarget. 2014;5:3785-99.
33. Georget V, Lobaccaro JM, Terouanne B, Mangeat P, Nicolas JC, C. S. Trafficking of the androgen receptor in living cells with fused green fluorescent protein-androgen receptor. Mol Cell Endocrinol. 1997;129:17-26.
34. Brooke GN, C.L. B. The role of androgen receptor mutations in prostate cancer progression. . Current Genomics. 2009;10:18-25.
35. Karantanos T, Evans CP, Tombal B, Thompson TC, Montironi R, Isaacs WB. Understanding the mechanisms of androgen deprivation resistance in prostate cancer at the molecular level. Eur Urol. 2015;67:470-9.
36. Park HU, Suy S, Danner M, Dailey V, Zhang Y, Li H, et al. AMP-activated protein kinase promotes human prostate cancer cell growth and survival. Mol Cancer Ther 2009;8:733–41.
37. Xiang X, Saha AK, Wen R, Ruderman NB, Luo Z. AMP-activated protein kinase activators can inhibit the growth of prostate cancer cells by multiple mechanisms. Biochem Biophys Res Commun. 2004;321(1):161-7.
38. Bain J, Plater L, Elliott M, Shpiro N, Hastie CJ, McLauchlan H, et al. The selectivity of protein kinase inhibitors: a further update. Biochem J. 2007;408:297-315.
39. Tennakoon JB, Shi Y, Han JJ, Tsouko E, White MA, Burns AR, et al. Androgens regulate prostate cancer cell growth via an AMPK-PGC-1alpha-mediated metabolic switch. Oncogene. 2014;33(45):5251-61.
40. Zadra G, Photopoulos C, Loda M. The fat side of prostate cancer. Biochim Biophys Acta. 2013;1831:1518-32.
41. Hsieh AC, Liu Y, Edlind MP, Ingolia NT, Janes MR, Sher A, et al. The translational lanscape of mTOR signalling steers cancer initiation and metastasis. Nature. 2012;485:55-61.
42. Lin F, Marcelo KL, Rajapakshe K, Coarfa C, Dean A, Wilganowski N, et al. The CaMKK2/CaMKIV relay is an essential regulator of hepatic cancer. Hepatology. 2015;62:505-20.

43. Wayman GA, Lee YS, Tokumitsu H, Silva AJ, Soderling TR. Calmodulin-kinases: modulators of neuronal development and plasticity. Neuron. 2008;59:914-31.
44. Srivastava T, Fortin DA, Nygaard S, Kaech S, Sonenberg N, Edelman AM, et al. Regulation of neuronal mRNA translation by CaM-kinase 1 phosphorylation of eIFGII. J Neurosci. 2012;32:5620-30.
45. Gocher AM, Azabdaftari G, Euscher LM, Dai S, Karacosta LG, Franke TF, et al. Akt activation by Ca2+/calmodulin-dependent protein kinase kinase 2 (CaMKK2) in ovarian cancer cells. J Biol Chem. 2017;292:14188-204.
46. Chen M, Zhang J, Sampieri K, Clohessy JG, Mendez L, Gonzalez-Billalabeitia E, et al. An aberrant SREBP-dependent lipogenic program promotes metastatic prostate cancer. Nat Genet. 2018;50:206-18.
47. Chen J, Guccini I, Mitri DD, Brina D, Revandkar A, Sarti M, et al. Compartmentalized activities of the pyruvate dehydrogenase complex sustain lipogenesis in prostate cancer. Nat Genet. 2018;50:219-28.
48. Sadowski MC, Pouwer RH, Gunter JH, Lubik AA, Quinn RJ, Nelson CC. The fatty acid synthase inhibitor triclosan: repurposing an anti-microbial agent for targeting prostate cancer. Oncotarget. 2014;5:9362-81.
49. Nakanishi A, Hatano N, Fujiwara Y, Sha'ri A, Takabatake S, Akano H, et al. AMP-activated protein kinase-mediated feedback phosphorylation controls the Ca2+/calmodulin (CaM) dependence of Ca2+/CaM-dependent protein kinase kinase β. J Biol Chem. 2017;292:13802-8.
50. Cameron KO, Kung DW, Kalgutkar AS, Kurumbail RG, Miller R, Salatto CT, et al. Discovery and preclinical characterization of 6-chloro-5-[4-(1- hydroxycyclobutyl)phenyl]-1H-indole-3-carboxylic acid (PF-06409577), a direct activator of adenosine monophosphate-activated protein kinase (AMPK), for the potential treatment of diabetic nephropathy. J Med Chem. 2016;59:8068-81.

Table 1. Proteins identified by mass spectrometry with significantly changed expression in anterior lobe of prostate tissue from *Pten;Camkk2* vs *Pten* mice.

Down-regulated in *Pten;Camkk2* vs *Pten*

Protein ID	Fold change	*P*-value
Abcf2	>10	0.0027
Fam98b	>10	0.0036
Vps25	>10	0.0053
Cyb5b	>10	0.0079
Egf	>10	0.0087
Tial1	>10	0.0098
Hnrnpll	>10	0.0124
Apmap	>10	0.0174
Gsdma	>10	0.0182
Gcat	>10	0.0268
Atp5j2	7.56	0.0196
Vdac2	6.08	0.0428
Ly6c1	5.33	0.0424
Usp9x	4.77	0.0443
Eif4a2	**3.52**	**0.0368**
Gne	3.49	0.0013
Papss2	3.01	0.0058
Eif3c	**2.99**	**0.0019**
Eif3e	**2.97**	**0.0019**
Dync1li2	2.91	0.0025
Copg1	2.83	0.0099
Eif4a1	**2.82**	**0.0099**
Golph3	2.77	0.0095
Fkbp5	2.77	0.0071
Fasn	2.76	0.0122
Eif3a	**2.64**	**0.0114**
Hsp90ab1	2.52	0.0106
Prkag1	2.46	0.0048
Cox4i1	2.45	0.0328
Vars	2.43	0.0344
Tmed7	2.40	0.0221
Cyfip1	2.35	0.0388
Hsp90aa1	2.34	0.0141
Hsp90b1	2.34	0.0065
Sec23b	2.29	0.0266
Stat1	2.23	0.0328
Ddx3x	2.21	0.0055
Tmed2	2.20	0.0040
Sec31a	2.18	0.0123
Asna1	2.18	0.0011
Dnajc10	2.17	0.0273
Ube2k	2.14	0.0043
Qars	2.12	0.0216
Gstm7	2.10	0.0210
Cox6b1	2.09	0.0484
Bpnt1	2.07	0.0164
Pdia6	2.07	0.0055
Papss1	2.06	0.0017
Kpnb1	2.03	0.0065
Apoa2	2.03	0.0469
Dync1li1	2.03	0.0041

Up-regulated in *Pten;Camkk2* vs *Pten*

Protein ID	Fold change	*P*-value
Pklr	>10	0.0002
Aif1	>10	0.0002
Wdr77	>10	0.0077
Endod1	>10	0.0079
H2afy	>10	0.0128
Mycbp	>10	0.0146
Cadm1	>10	0.0220
Pqbp1	>10	0.0304
Dbn1	6.84	0.0116
Pvrl2	4.89	0.0392
Lin7c	4.84	0.0405
Hspa1b	4.61	0.0476
F11r	4.30	0.0136
Hist1h1e	2.59	0.0163
Lmnb1	2.56	0.0437
H1f0	2.54	0.0121
Clca1	2.34	0.0238
H2afv	2.20	0.0406
S100a16	2.09	0.0444
Ltbp2	2.09	0.0044
Hist1h1d	2.06	0.0361
Fbl	2.02	0.0233
Mpst	2.02	0.0340

Protein lysates from the anterior prostate lobes of three independent animals per genotype aged 17 weeks were analysed in duplicated. Proteins with a fold change >2 and $P<0.05$ were determined to be significantly changed. Fasn is highlighted in grey and eukaryotic translation initiation factors in bold text.

FIGURE LEGENDS

Figure 1. Camkk2 deletion protects against prostate cancer development in the *Pten* prostate cancer mouse model. (A) *Camkk2* mRNA from wild-type (WT), *Pten* and *Pten;Camkk2* prostate of mice aged 17 weeks (n=5-7 mice per genotype) was determined. Significant difference between WT and *Pten* null mice is shown; ****P<0.0001. (B) Representative Western blot showing Camkk2 expression in prostates from wild-type (WT), *Pten* and *Pten;Camkk2* mice aged 17 weeks together with graph of quantification. *P<0.05 significant difference in expression between WT and Pten null samples (n=5-7 mice per genotype). (C) Wet weight of whole prostate relative to bodyweight (n=7-15 per genotype). **P<0.01, ***P<0.005 significant differences between genotypes. (D) Quantification of pathological grading from 26 week old mice. A range of PIN grades were found within a prostate section and so may appear in more than one category (n=10 for *Pten* and 8 for *Pten;Camkk2* mice). Significant differences using Fisher's exact test (two sided *P* value) are indicated as *P<0.05 and ****P<0.0001. (E) Percentage of Ki-67-positive cells in prostate sections of 26 week old mice (n=3-4 mice for each genotype; 5,000 cells per lobe). ***P<0.005 significant differences between genotypes. (F) H+E stained sections from 40 week old mice were scored for adenocarcinoma (n=5-6 per genotype). Two sided *P* value using Fisher's exact test is 0.06.

Figure 2. Effect of STO-609 in the *Pten* prostate cancer mouse model. (A) Steady-state levels of plasma STO-609. (B) Tissue levels after 4 weeks treatment with 30 mg/ml STO-609. Data for (A) and (B) are means ± SEM (n=3). (C) Wet weight of prostate normalised to body weight following 6 weeks of STO-609 treatment (n=7-8 mice for each condition). Data are means ± SEM; **P<0.01. (D) Representative images of anterior prostate lobe from vehicle and STO-609 treated mice. (E) Quantification of pathological grading from vehicle and STO-609 treated mice. The graph shows the highest grade lesion observed in each prostate section (n=5 mice per condition).

Figure 3. Ampkβ1 deletion accelerates prostate cancer development in the *Pten* null prostate cancer mouse model. (A) Western blot analysis of Ampk subunits in lysates from anterior lobes of prostates isolated from wild-type (WT), *Camkk2*, *Pten* and *Pten;Camkk2* mice aged 17 weeks. (B) Western blot analysis from wild-type (WT), *Pten* and *Pten;Prkab1* mice aged 12 weeks. Quantification is shown underneath the respective blots. Expression was normalised to β-actin, and values shown are fold changes relative to expression in the WT tissue. Significant differences between WT and *Pten* samples are shown as *P<0.05, **P<0.01, ****P<0.0001, and between *Pten* and *Pten;Camkk2* or *Pten;Prkab1* are shown as ####P<0.0001. No significant differences were observed between WT and *Camkk2* prostate tissue. (C) Prostate wet weight normalised to bodyweight (n=7-15 mice per genotype). Data are

means ± SEM; ns: no significant difference. (D) Quantification of pathological grading from 26 week old mice. A range of PIN grades were found within a prostate section and so appear in more than one category (n=7-10 per genotype). Significant difference using Fisher's exact test (two sided *P* value) between genotypes is shown, **P*<0.05. (E) Percentage of Ki-67-positive cells in prostate sections of 26 week old mice. (n=3-4 mice for each genotype; 5,000 cells per lobe). Data are presented as mean ± SEM, **P*<0.05. (F) Representative images of Ki-67 stained sections for each genotype are shown.

Figure 4. Camkk2 deletion downregulates *de novo* lipogenesis. (A) Western blot analysis of acetyl-CoA carboxylase 1 (Acc1) and fatty acid synthase (Fasn) in lysates from the anterior lobe of prostates isolated from wild-type (WT), *Camkk2*, *Pten* and *Pten;Camkk2* mice aged 17 weeks, and quantification is shown. Values shown are fold changes relative to expression in the WT tissue. Data are means ± SEM (n=6 mice per genotype) and significant differences from WT are shown as **P*<0.05, ****P*<0.005, and between *Pten* and *Pten;Camkk2* as ##*P*<0.01, ###*P*<0.005. **P*<0.05, ****P*<0.005 relative to wild-type; ##*P*<0.01 relative to *Pten* null genotype. (B) *Acc1* and *Fasn* mRNA expression in wild-type (WT), *Pten* and *Pten;Camkk2* mice aged 17 weeks. Data are means ±SEM (n=5-7 mice per genotype). *P<0.05, ***P*<0.01, ns, not significant. (C) Wild-type (WT) and CAMKK2 KO (KO) LNCaP cells were treated ± mibolerone (Mib; 1 nM) and ± 991 (15 μM) for 24 h and ACC1, FASN, and CAMKK2 protein expression determined. Quantification of the data is show alongside the blot. Values shown are fold changes relative to expression in vehicle treated WT cells. Data are means ± SEM of 5-8 independent experiments and significant differences are shown as ***P*<0.01, *****P*<0.0001. (D) Incorporation of ^{3}H-acetate into lipids, following treatment of WT and CAMKK2 KO LNCaP cells with mibolerone (1 nM) and/ or 991 (10 μM) for 24 hours. Data are means ± SEM (n=5). Significant differences between WT and CAMKK2 KO cells under the same conditions are shown as **P*<0.05, *****P*<0.0001; differences between vehicle treated WT and WT treated are shown as ####*P*<0.0001; $$$$*P*<0.0001. (E) WT and CAMKK KO LNCaP cells were grown in the presence of mibolerone (1 nM) ± 991 (15 μM) and ± palmitic acid (PA). Relative cell growth was measured after 3 days. Data shown are the means ±SEM (n=5 independent experiments, 6 replicates per experiment) and plotted relative to cell growth in the vehicle treated WT cells. Significant differences to vehicle treated WT cells are shown as ***P*<0.001, *****P*<0.0001 and between cells grown in the absence of PA compared to the presence of PA, ##*P*<0.001 and ####$_{P}$<0.0001.

Figure 5. Effect of AMPK activation on human prostate cancer cell proliferation, migration and invasion. (A) LNCaP cells treated for 16 h with varying concentrations of 991

and phosphorylation of AMPK (T172) and ACC1 (S79) determined. (B) AMPK activity in immune complexes isolated from cells treated as in (A). Results were normalised to the DMSO control condition. Data are presented as fold activity relative to AMPK activity in the absence of 991 and are plotted as the mean ± SEM, ***P*<0.01, ****P*<0.005, significantly different between control and 20 μM 991 treated cells. (C) Cell proliferation in LNCaP, DU145, PC3 and 22Rv1 was measured over 16 h ±991 (10 μM). Results shown are relative to proliferation in the absence of 991. ****P*<0.005 shows significant differences between control and 991 treated cells. (D) Cell cycle analysis of DU145 and PC3 cells grown ±991 (10 μM). Data are means ± SEM (n=3), ***P*<0.01 significantly different between vehicle and 991 treated cells. (E) Cell viability was measured ±991 (10 μM). Data shown are the means ±SEM for 6 samples per condition; ns, not significant. (F) Migration of 22Rv1 cells was measured over 12 h ± varying concentrations of 991. Below the graph, representative images are shown for 0 and 10 μM 991. (G) Invasion of 22Rv1 cells was measured ± 991 (10 μM). Results shown are the invasion rates measured from 30 to 60 h after plating the cells and are plotted relative to the invasion rate measured in the absence of 991. Data shown in (F) and (G) are means ±SEM (n=4), ***P*<0.01, ****P*<0.005.

Figure 6. Activation of AMPK significantly inhibits androgen signalling in LNCaP cells. (A) Western blot analysis of ACC1 (S79) and AMPK (T172) phosphorylation in wild-type (WT) and CAMKK2 KO LNCaP cells treated with mibolerone (Mib; 1 nM) for 24 h. Quantification of phosphorylation shown. (B) LNCaP cells were treated with vehicle, mibolerone (1 nM), or mibolerone (1 nM) and 991 (10 μM) for 24 h. Androgen receptor (AR) expression in the cytosolic and nuclear fractions was determined. AR expression was normalised to β-actin (cytosolic) or histone H3 (nuclear). Values for AR expression are indicated on the blots, and are shown relative to the non-treated condition for cytosolic samples and the mibolerone treated condition for the nuclear samples; nd, not determined. (C) Expression of AR-regulated genes (*CAMKK2*; *PSA*, prostate specific antigen*; TMPRSS2*, transmembrane protease, serine 2; *FKBP5*, FK506 binding protein 5) in LNCaP cells treated ± mibolerone (1 nM), ± 991 (10 μM), for 24 h is shown. Results shown are means ±SEM (n=5), significant differences from vehicle control are shown as ***P*<0.01, ****P*<0.005; ###*P*<0.005 between mibolerone alone and mibolerone + 991 treated cells. (D) Model showing opposing role of CAMKK2 and AMPK in prostate cancer progression.

Figure 1

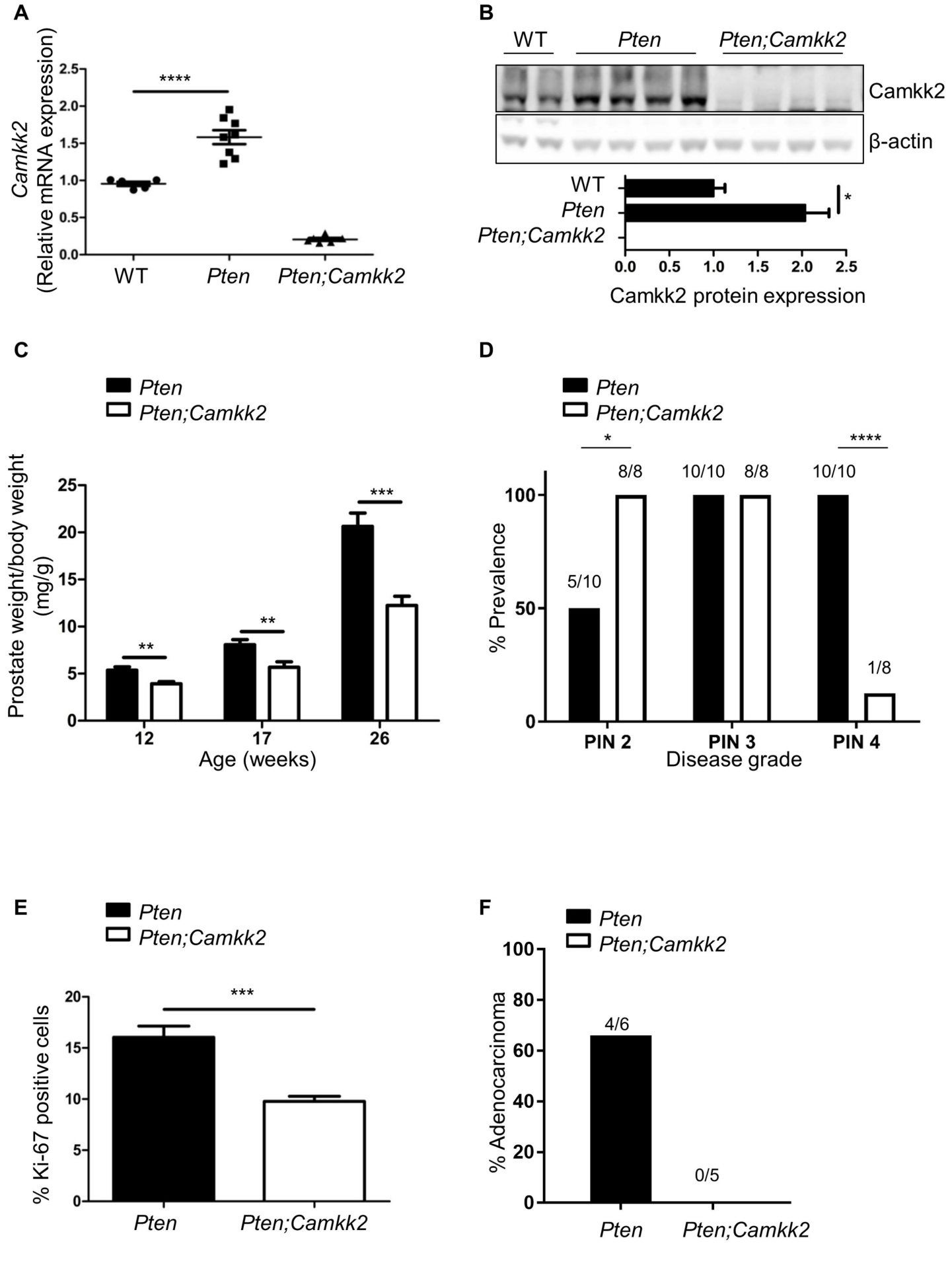
A
Camkk2
(Relative mRNA expression)
2.5
2.0
1.5
1.0
0.5
0.0
****
WT
Pten
Pten;Camkk2
B
WT
Pten
Pten;Camkk2
Camkk2
β-actin
WT
Pten
Pten;Camkk2
*
0.0
0.5
1.0
1.5
2.0
2.5
Camkk2 protein expression
C
Pten
Pten;Camkk2
Prostate weight/body weight
(mg/g)
25
20
15
10
5
0
**
**
***
12
17
26
Age (weeks)
D
Pten
Pten;Camkk2
*
****
8/8
10/10
8/8
10/10
100
50
0
% Prevalence
5/10
1/8
PIN 2
PIN 3
PIN 4
Disease grade
E
Pten
Pten;Camkk2
% Ki-67 positive cells
20
15
10
5
0
***
Pten
Pten;Camkk2
F
Pten
Pten;Camkk2
100
80
60
40
20
0
% Adenocarcinoma
4/6
0/5
Pten
Pten;Camkk2

Figure 2

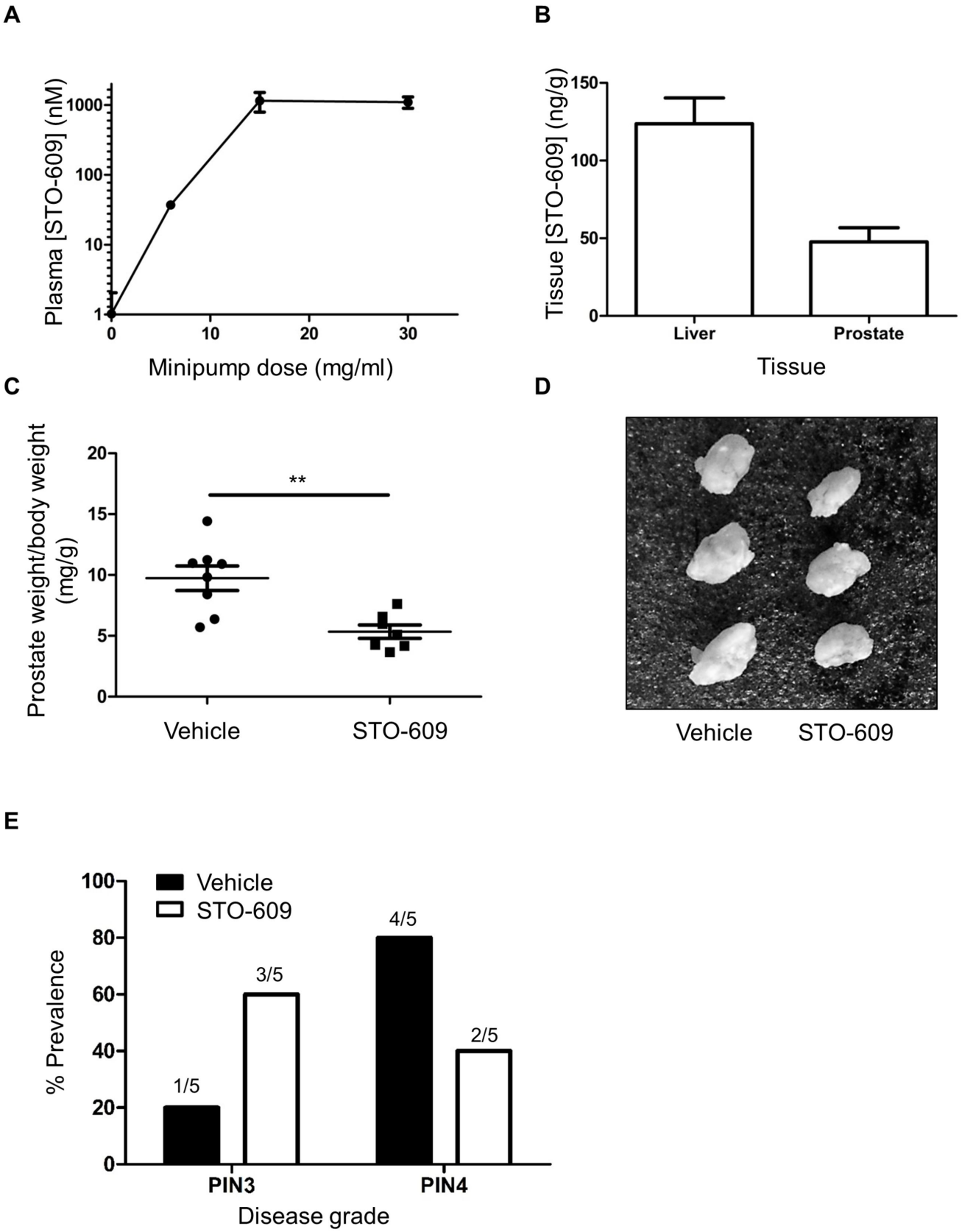
A
Plasma [STO-609] (nM)
1000
100
10
1
0
10
20
30
Minipump dose (mg/ml)
B
Tissue [STO-609] (ng/g)
150
100
50
0
Liver
Prostate
Tissue
C
Prostate weight/body weight (mg/g)
20
15
10
5
0
**
Vehicle
STO-609
D
Vehicle
STO-609
E
% Prevalence
100
80
60
40
20
0
Vehicle
STO-609
1/5
3/5
4/5
2/5
PIN3
PIN4
Disease grade

Figure 3

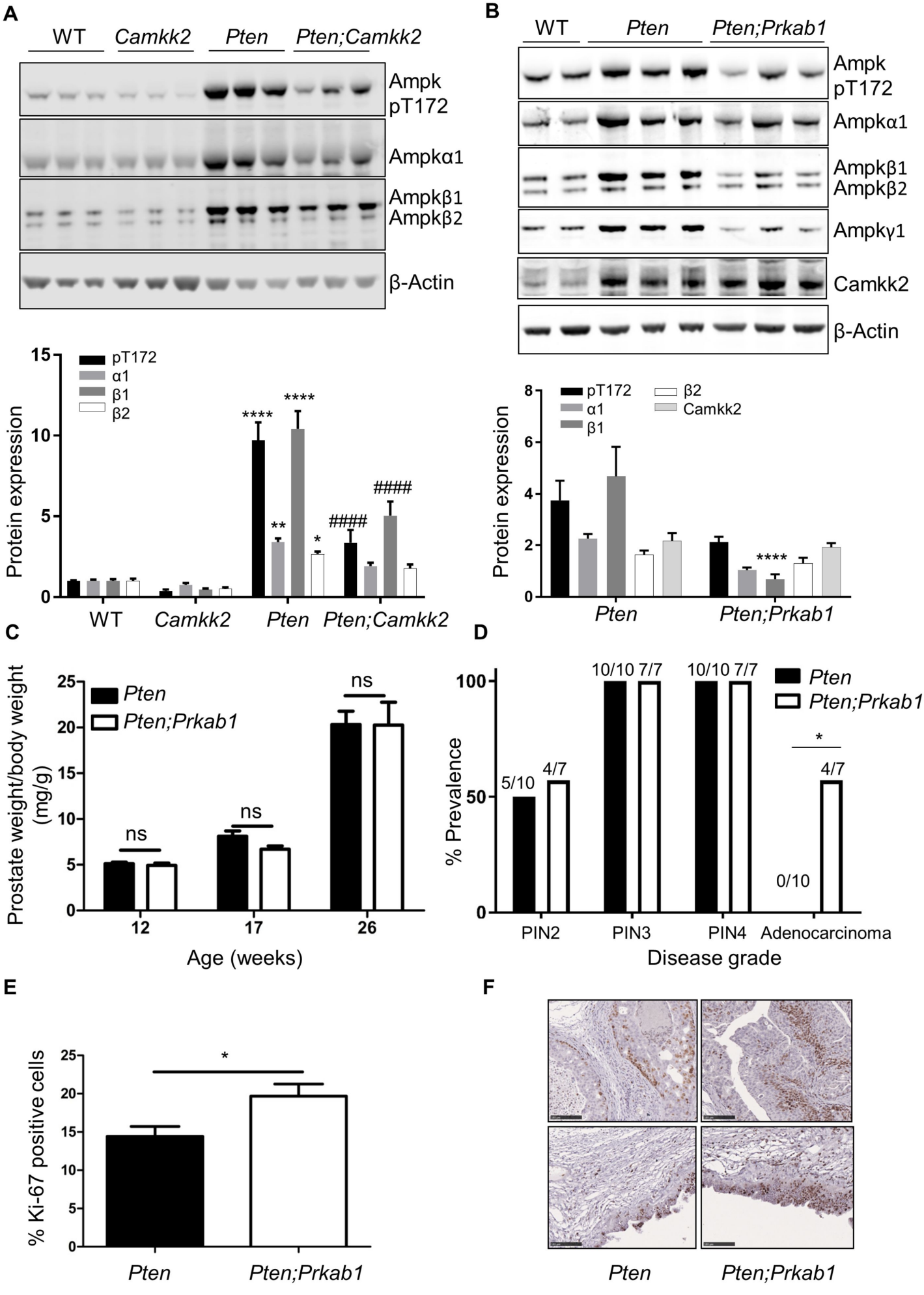
A
WT
Camkk2
Pten
Pten;Camkk2
Ampk pT172
Ampkα1
Ampkβ1
Ampkβ2
β-Actin
B
WT
Pten
Pten;Prkab1
Ampk pT172
Ampkα1
Ampkβ1
Ampkβ2
Ampkγ1
Camkk2
β-Actin
Protein expression
pT172
α1
β1
β2
****
**
*
####
WT
Camkk2
Pten
Pten;Camkk2
Protein expression
pT172
α1
β1
β2
Camkk2
****
Pten
Pten;Prkab1
C
Prostate weight/body weight (mg/g)
Pten
Pten;Prkab1
ns
ns
ns
12
17
26
Age (weeks)
D
% Prevalence
Pten
Pten;Prkab1
10/10 7/7
10/10 7/7
5/10
4/7
*
4/7
0/10
PIN2
PIN3
PIN4
Adenocarcinoma
Disease grade
E
% Ki-67 positive cells
*
Pten
Pten;Prkab1
F
Pten
Pten;Prkab1

Figure 4

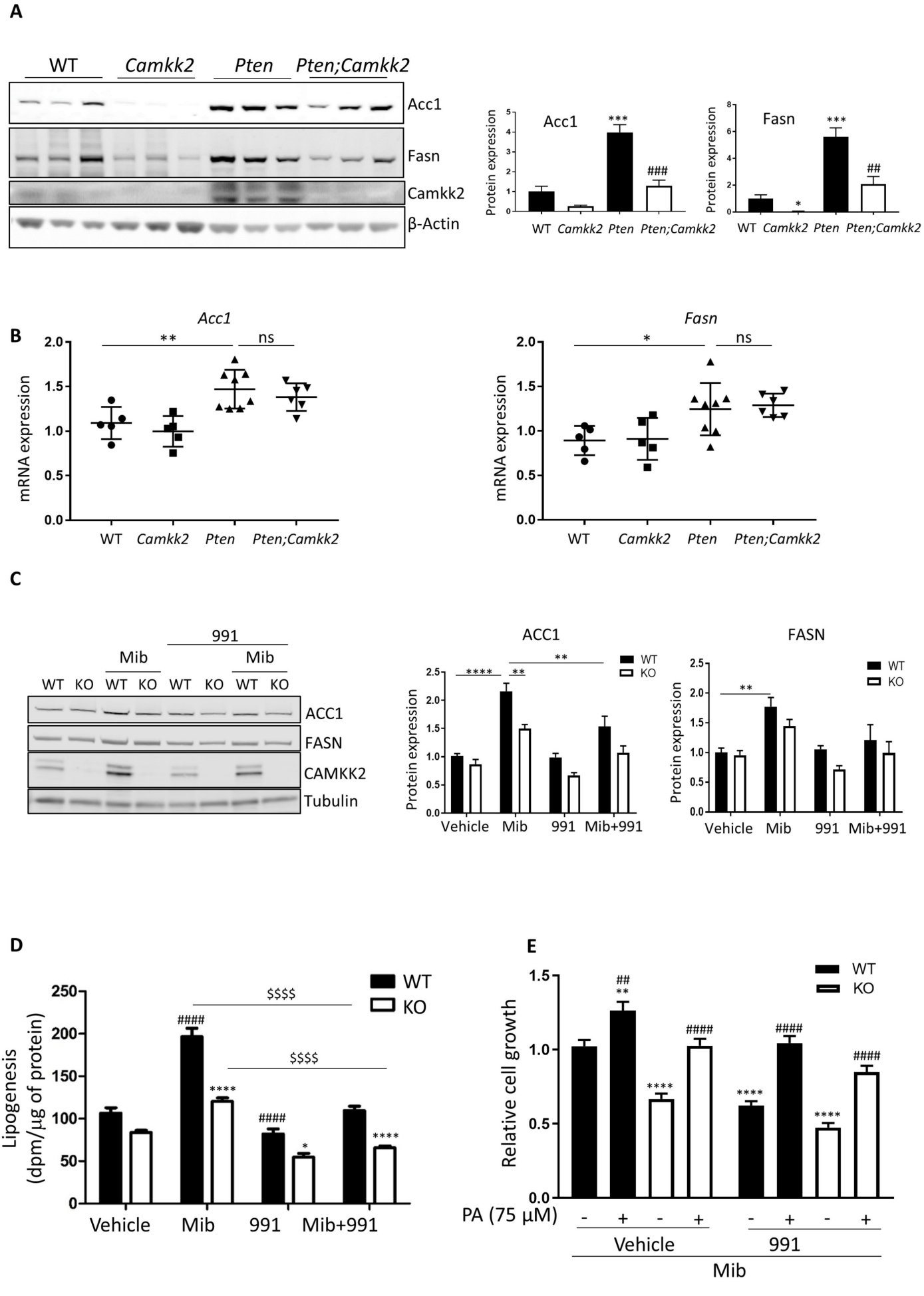
A
WT
Camkk2
Pten
Pten;Camkk2
Acc1
Fasn
Camkk2
β-Actin
Protein expression
Acc1
Fasn
***
###
##
*
WT Camkk2 Pten Pten;Camkk2
B
Acc1
Fasn
mRNA expression
**
*
ns
WT Camkk2 Pten Pten;Camkk2
C
991
Mib
Mib
WT KO WT KO WT KO WT KO
ACC1
FASN
CAMKK2
Tubulin
ACC1
FASN
Protein expression
WT
KO
****
**
Vehicle Mib 991 Mib+991
D
Lipogenesis (dpm/μg of protein)
WT
KO
$$$$
$$$$
####
****
Vehicle Mib 991 Mib+991
E
Relative cell growth
PA (75 μM)
Vehicle
991
Mib

Figure 5

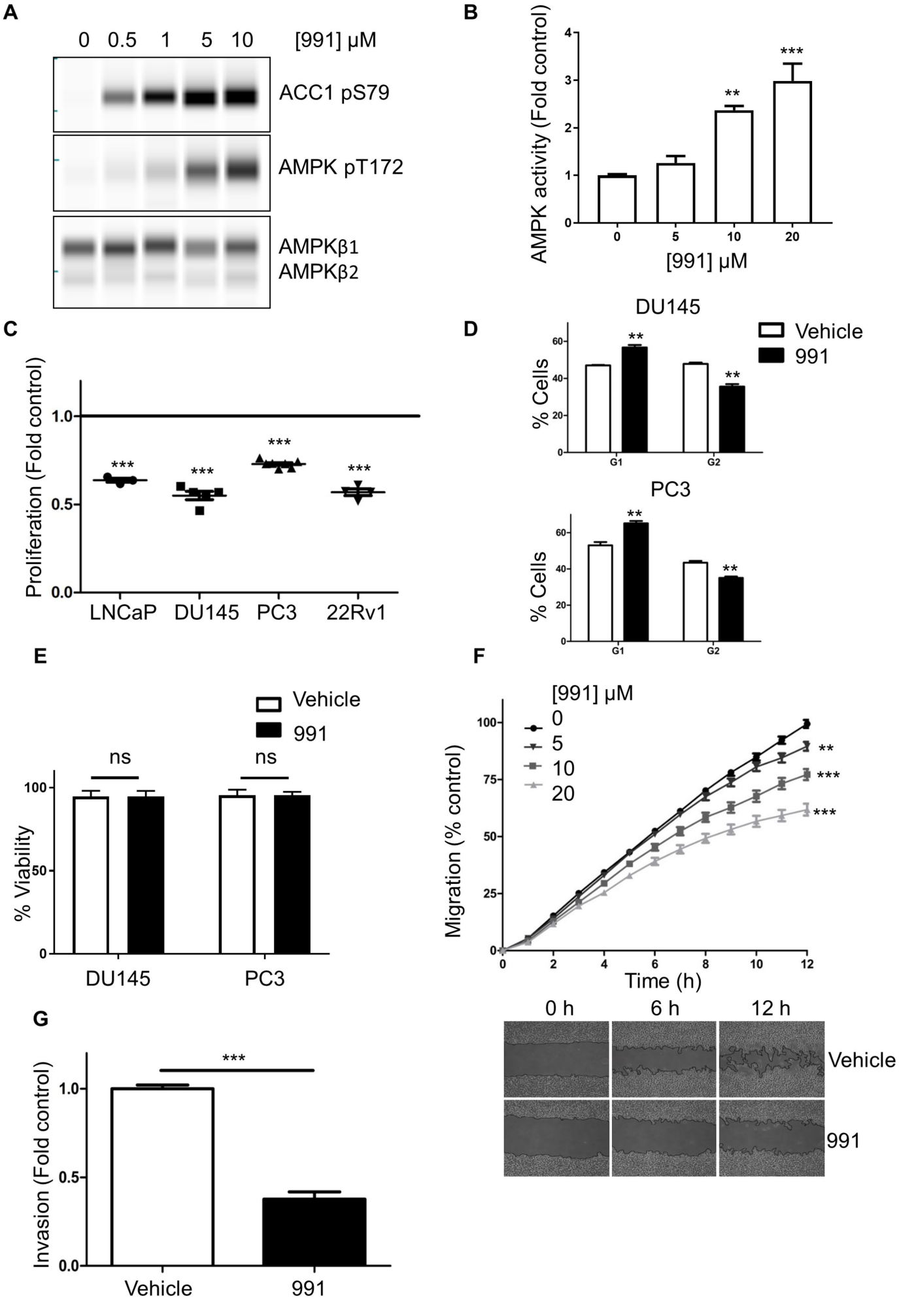
A
0 0.5 1 5 10 [991] μM
ACC1 pS79
AMPK pT172
AMPKβ1
AMPKβ2
B
AMPK activity (Fold control)
[991] μM
C
Proliferation (Fold control)
LNCaP DU145 PC3 22Rv1
D
DU145
PC3
% Cells
Vehicle
991
G1
G2
E
% Viability
Vehicle
991
ns
DU145
PC3
F
[991] μM
0
5
10
20
Migration (% control)
Time (h)
0 h
6 h
12 h
Vehicle
991
G
Invasion (Fold control)
Vehicle
991

Figure 6

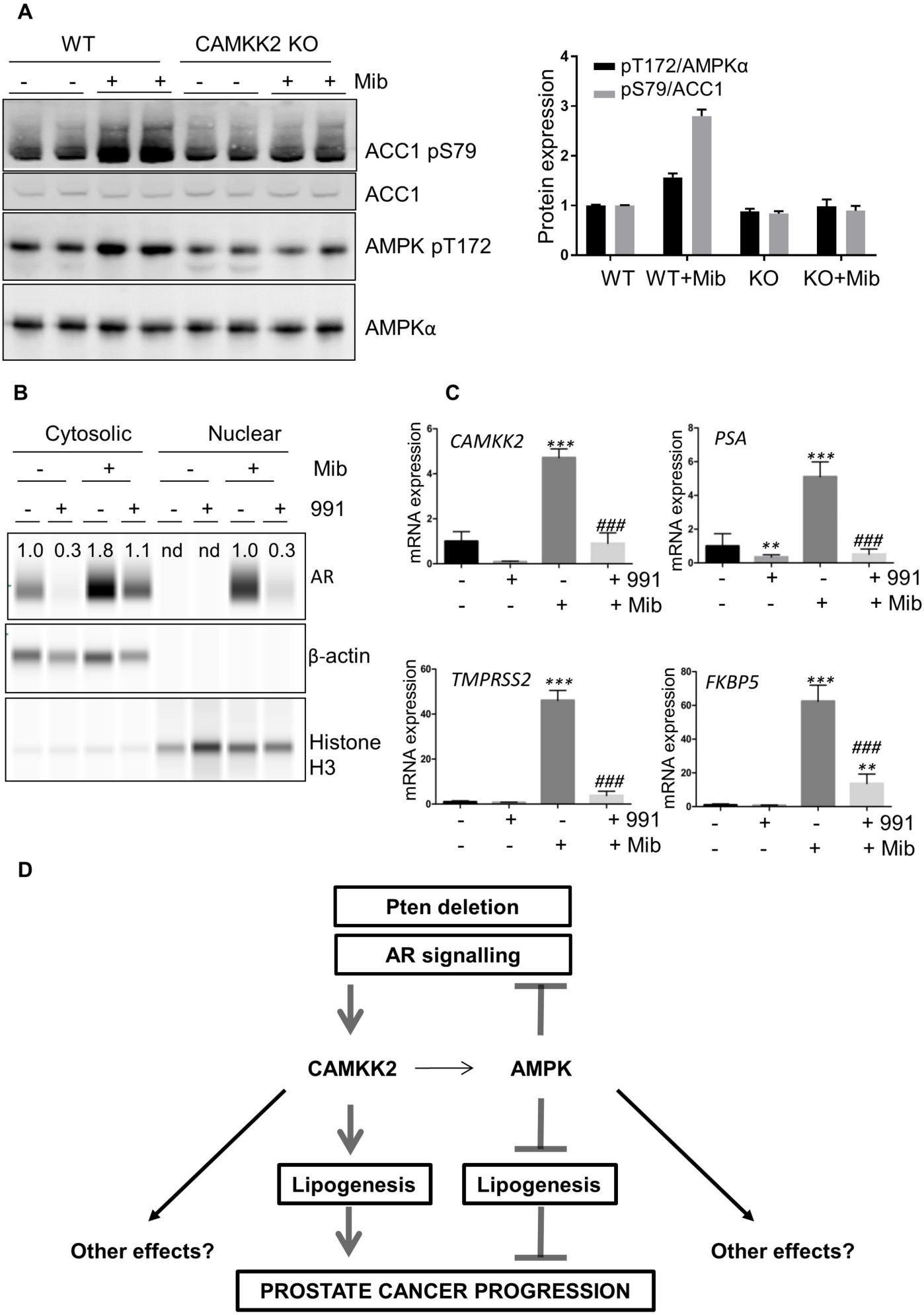
A
WT
CAMKK2 KO
- - + + - - + + Mib
ACC1 pS79
ACC1
AMPK pT172
AMPKα
pT172/AMPKα
pS79/ACC1
Protein expression
WT WT+Mib KO KO+Mib
B
Cytosolic
Nuclear
Mib
991
1.0 0.3 1.8 1.1 nd nd 1.0 0.3
AR
β-actin
Histone H3
C
CAMKK2
PSA
TMPRSS2
FKBP5
mRNA expression
+ 991
+ Mib
D
Pten deletion
AR signalling
CAMKK2
AMPK
Lipogenesis
Lipogenesis
Other effects?
Other effects?
PROSTATE CANCER PROGRESSION